KIAA1429 knockdown alleviates osteosarcoma progression by destabilizing SLC7A11 mRNA via m6A methylation to promote ferroptosis

HUI ZENG[1], YUNYAN ZHONG[2], DINGBIAO ZENG[1], SHILIANG XIAO[1] and SONG ZOU[3]

[1]Department of Orthopedics, Ganzhou People's Hospital, Ganzhou, Jiangxi 341000, P.R. China;
[2]Department of Medical Records, Ganzhou People's Hospital, Ganzhou, Jiangxi 341000, P.R. China;
[3]Department of Interventional Radiology and Vascular Surgery, Ganzhou Key Laboratory of Interventional Medicine, Ganzhou Hospital-Nanfang Hospital, Southern Medical University (Ganzhou People's Hospital), Ganzhou, Jiangxi 341000, P.R. China

Received November 10, 2025; Accepted May 28, 2026

DOI: 10.3892/ijo.2026.5929

Abstract. Osteosarcoma (OS) is a highly aggressive bone tumor with limited therapeutic options. As a key component of the N6-methyladenosine (m6A) methyltransferase complex, KIAA1429 contributes to tumor progression; however, its role in OS remains unclear. For the present study, four human OS cell lines (MG63, 143B, U2OS and Saos-2) and an osteoblast cell line (hFOB1.19) were cultured *in vitro*, and KIAA1429 was knocked down in 143B and U2OS cells. To evaluate functional effects, cell proliferation was assessed using a Cell Counting Kit-8 assay, apoptosis was evaluated by flow cytometry, migration was assessed by Transwell assay and invasion was analyzed using a wound healing assay. Subsequently, ferroptosis was induced using erastin, and analyzed by western blotting, ELISA, C11-BODIPY staining and m6A-modified RNA immunoprecipitation-quantitative PCR. In addition, actinomycin D was used to inhibit transcription and to assess mRNA stability. The interaction between KIAA1429 and solute carrier family 7 member 11 (SLC7A11) was validated using a dual-luciferase reporter assay. Furthermore, a xenograft model was established in BALB/c nude mice to assess tumor growth and ferroptosis markers, and tumor histology and proliferation were examined using hematoxylin and eosin staining and immunohistochemistry. The results revealed that KIAA1429 was significantly upregulated in OS cells, whereas its knockdown markedly suppressed malignant cellular behaviors. Downregulation of KIAA1429 also enhanced erastin-induced ferroptosis. Mechanistically, KIAA1429 knockdown reduced m6A modification and decreased the stability of SLC7A11 mRNA, leading to its downregulation. Rescue experiments demonstrated that SLC7A11 overexpression reversed the effects of KIAA1429 knockdown on ferroptosis and malignant phenotypes. *In vivo*, KIAA1429 knockdown inhibited tumor growth and promoted ferroptosis, effects that were reversed by SLC7A11 overexpression. In conclusion, KIAA1429 knockdown may suppress OS progression by inhibiting m6A-dependent SLC7A11 expression, thereby promoting ferroptosis. Targeting the KIAA1429/SLC7A11 axis may thus represent a promising therapeutic strategy for OS.

Introduction

Osteosarcoma (OS), which predominantly affects young individuals during periods of rapid bone growth, is the most common primary malignant bone tumor and shows a marked increase in incidence during adolescence (1). Due to its aggressive local invasion and high metastatic potential, OS is associated with a poor prognosis, with a 5-year survival rate of <20% in patients with metastatic disease worldwide (2,3). The current therapeutic regimen focuses on surgical intervention complemented by adjuvant chemotherapy (4). Nevertheless, clinical outcomes remain unsatisfactory for recurrent and refractory OS, which is attributed to rapid disease progression and inherent chemoresistance (5). Amid the evolving landscape of oncological therapeutics, molecularly targeted approaches have emerged as a promising frontier in the management of OS.

KIAA1429, a component of the RNA methyltransferase complex, regulates N6-methyladenosine (m6A) modification of mRNA, influencing RNA stability, splicing and translation (6). In cancer, KIAA1429 is upregulated and acts as an oncogene by promoting cell proliferation, migration and invasion (6,7). Through an m6A-YTH domain family protein 2-mediated mechanism, KIAA1429 exerts its oncogenic role in gastric cancer progression by inducing the destabilization of dexamethasone-induced Ras-related protein 1 mRNA (8). As a constituent of the m6A methyltransferase complex, KIAA1429 is elevated in breast cancer specimens and is positively associated with reduced patient survival (9). Elevated

Correspondence to: Dr Song Zou, Department of Interventional Radiology and Vascular Surgery, Ganzhou Key Laboratory of Interventional Medicine, Ganzhou Hospital-Nanfang Hospital People's Hospital, Southern Medical University (Ganzhou People's Hospital), 16 Meiguan Avenue, Ganzhou, Jiangxi 341000, P.R. China
E-mail: z13879757375@163.com

Key words: osteosarcoma, KIAA1429, ferroptosis, N6-methyladenosine methylation, solute carrier family 7 member 11

KIAA1429 expression is also associated with unfavorable clinical outcomes and increased disease aggressiveness in OS (10). These findings suggest that KIAA1429 is a promising therapeutic target for OS.

Ferroptosis is a crucial pathway in cancer biology, characterized by iron-dependent lipid peroxidation that drives this distinct form of regulated cell death (11). Its molecular signature includes the suppression of glutathione (GSH) peroxidase 4 (GPX4) and the consequent accumulation of reactive oxygen species (ROS) (12). Notably, induction of ferroptosis has emerged as a promising therapeutic strategy for OS (13); therefore, elucidating the molecular mechanisms underlying ferroptosis in OS may help overcome the limitations of conventional treatments. Solute carrier family 7 member 11 (SLC7A11) is a key component of the system Xc^- cystine/glutamate antiporter and serves a crucial role in maintaining intracellular redox homeostasis by facilitating cystine uptake and GSH biosynthesis (14). Inhibition of SLC7A11 depletes GSH, thereby impairing cellular antioxidant capacity and promoting ROS accumulation, ultimately sensitizing cells to ferroptosis (15). A previous study demonstrated that compounds such as erastin and brusatol induce ferroptosis by suppressing the kelch-like ECH-associated protein 1/nuclear factor erythroid 2-related factor 2 (Nrf2)/SLC7A11 pathway, thereby inhibiting cystine uptake and enhancing ROS accumulation (16). Mechanistically, KIAA1429 silencing suppresses OS progression by promoting ferroptosis via the Nrf2/NAD(P)H quinone oxidoreductase 1 axis (17). Specifically, KIAA1429 directly targets the 3'UTR of Nrf2 mRNA through m6A modification, thereby inhibiting Nrf2 signaling and enhancing erastin-induced ferroptosis (17). While this previous study provides important insights (17), the present study offers several distinct advantages and novel findings. The current study aimed to investigate the role of KIAA1429 in OS progression and to determine whether it modulates ferroptosis via m6A-dependent regulation of SLC7A11 expression. Specifically, the study sought to elucidate the mechanistic relationship among KIAA1429, m6A methylation, SLC7A11 stability and ferroptosis in OS cells, and to validate this axis in an *in vivo* xenograft model.

Materials and methods

Cell culture and transfection. Human osteoblasts (hFOB1.19) and human OS cell lines (MG63, 143B, U2OS and Saos-2) were obtained from iCell Bioscience Inc., and were routinely cultured in Dulbecco's modified Eagle's medium (DMEM supplemented with 10% fetal bovine serum (FBS) (both from Gibco, Thermo Fisher Scientific) and 100 U/ml penicillin/streptomycin. The cells were maintained at 37˚C in a humidified atmosphere containing 5% CO_2.

For experiments involving 143B and U2OS cells, the groups were designated as follows: Control (untreated) and small interfering (si)RNA-negative control (NC; si-NC); three experimental groups targeting KIAA1429 (si-KIAA1429-1, si-KIAA1429-2 and si-KIAA1429-3); and a combined intervention group [si-KIAA1429 + SLC7A11 overexpression vector (oe-SLC7A11)]. All siRNAs were purchased from Shanghai GenePharma Co., Ltd. oe-SLC7A11 was constructed by cloning full-length SLC7A11 cDNA into the pcDNA3.1(+) vector (Invitrogen; Thermo Fisher Scientific, Inc.), and the empty pcDNA3.1(+) vector served as the oe-NC. The si-NC group served as the NC for siRNA transfection. Transfection was performed using Lipofectamine® 3000 (Invitrogen; Thermo Fisher Scientific, Inc.) according to the manufacturer's protocol. Briefly, the cells were seeded in 6-well plates and cultured until they reached 70-80% confluence at the time of transfection. For siRNA transfection, the final concentration of si-KIAA1429 or si-NC was 50 nM; for plasmid (oe-SLC7A11 or oe-NC) transfection, and plasmid and siRNA co-transfection, the final concentration of siRNA was 50 nM and the final concentration of plasmid was 100 nM. The transfection mixture was incubated with cells for 6 h at 37˚C, after which the medium was replaced with fresh complete DMEM containing 10% FBS. The cells were harvested for subsequent experiments 48 h after transfection siRNA sequences are presented in Table I. For ferroptosis induction, 143B and U2OS cells were treated with 10 μM erastin (Selleck Chemicals) for 24 h at 37˚C, whereas for transcriptional inhibition, actinomycin D (5 μg/ml; Selleck Chemicals) was applied followed by RNA collection at the indicated time points (0, 3 and 6 h after treatment).

Cell Counting Kit-8 (CCK-8) assay. The proliferation rates of 143B and U2OS cells were determined using a CCK-8 (MilliporeSigma) assay. Cells were seeded at $1.5x10^4$ cells/well in 96-well plates and maintained under controlled conditions (37˚C, 5% CO_2). At the indicated time points (24, 48, 72 and 96 h), the culture medium was carefully aspirated, and 10 μl CCK-8 reagent was added to each well. After incubation for 2 h at 37˚C in the dark, optical density (OD) values were measured at 450 nm using a microplate reader.

Flow cytometric analysis. Apoptosis was detected using an Annexin V-FITC/PI Apoptosis Detection Kit (BD Biosciences) according to the manufacturer's instructions. Adherent cells were washed twice with phosphate-buffered saline (PBS), dissociated with EDTA-free trypsin, neutralized and centrifuged at 300 x g for 5 min at 4˚C. The cells ($5x10^4$) were then resuspended in 195 μl Annexin V-FITC binding buffer. Subsequently, the cells were stained with 5 μl Annexin V-FITC and 10 μl propidium iodide, incubated for 10-20 min at 20-25˚C in the dark and then placed on ice. Apoptosis was analyzed using a flow cytometer (CytoFLEX; Beckman Coulter, Inc.). The data were processed using CytExpert software version 2.0 (Beckman Coulter, Inc.).

Transwell invasion assay. Cell invasion was assessed using 24-well Transwell inserts (Corning, Inc.) with an 8.0-μm pore size. Firstly, Matrigel (Corning, Inc.) was thawed on ice, diluted with serum-free DMEM (1:8 ratio) and 50 μl diluted Matrigel was added to the upper chamber of each insert. Matrigel-coated Transwell inserts (Corning, Inc.) were then incubated at 37˚C for 30 min to allow gelation, followed by rehydration with serum-free medium for 1 h at 37˚C. Trypsinized cells were washed, resuspended in serum-free medium containing 0.1% bovine serum albumin (BSA; MilliporeSigma) and seeded ($1x10^4$ cells/well) into the upper chamber. Complete medium containing 20% FBS was added to the lower chamber (600 μl/well) as a chemoattractant. After incubation for 24 h

(37˚C, 5% CO_2), non-invasive cells on the upper surface of the membrane were removed using a cotton swab. Invasive cells on the lower surface were fixed with 4% paraformaldehyde for 30 min and stained with 0.1% crystal violet for 20 min at 37˚C, before images were captured under an inverted light microscope (CKX53; Olympus Corporation) and invasion was semi-quantified using ImageJ software (version 1.54; National Institutes of Health).

Wound healing assay. Cell migration was assessed using a standard wound healing assay. Briefly, 143B and U2OS cells were cultured in 6-well plates until they reached ~80% confluence. The cell monolayer was then carefully scratched in a straight line using a sterile 200-μl pipette tip held perpendicular to pre-marked horizontal lines on the plate; the wound width was kept consistent across all samples. After scratching, the detached cells were removed by washing with PBS, and serum-free medium was added to minimize cell proliferation. Images of the wounds were captured at 0 and 24 h post-scratching using a light microscope. The migration rate was semi-quantified by measuring changes in the wound area using ImageJ software (version 1.54).

Reverse transcription-quantitative PCR (RT-qPCR). Total RNA was extracted from cells using TRIzol® reagent (Invitrogen; Thermo Fisher Scientific, Inc.). A 5-μl aliquot of the total RNA was diluted with RNase-free ultrapure water, and RNA concentration and purity were assessed by measuring absorbance at 260 and 280 nm using a UV spectrophotometer. Samples with an OD260/OD280 ratio between 1.9 and 2.0 were considered to have high purity and were suitable for subsequent experiments. RT was performed using the PrimeScript™ RT Master Mix (Takara Bio, Inc.) according to the manufacturer's protocol. qPCR was conducted using the TB Green® Premix Ex Taq™ II (Tli RNaseH Plus) (Takara Bio, Inc.) on an ABI 7500 Real-Time PCR System (Applied Biosystems; Thermo Fisher Scientific, Inc.) under the following conditions: Initial denaturation at 95˚C for 30 sec, followed by 40 cycles of denaturation at 95˚C for 10 sec and annealing at 60˚C for 30 sec. GAPDH was used as the internal reference gene. Relative gene expression levels were calculated using the $2^{-\Delta\Delta Ct}$ method (18). Primer sequences are listed in Table I.

ELISA. The levels of oxidative stress and iron metabolism markers, including malondialdehyde (MDA) (cat no. YX-130401H for OS cells, cat no. EK20347 for tumor tissues), Fe^{2+} (cat no. YX-0605H for OS cells, cat no. EK20235 for tumor tissues), GSH (cat no. YX-071908H for OS cells, cat no. EK20064 for tumor tissues) and ROS (cat no. YX-202403H for OS cells, cat no. EK202408 for tumor tissues), in cells and tumor tissues were measured using specific commercial ELISA kits (Shanghai Yixuan Biotechnology Co., Ltd.) in accordance with the manufacturer's instructions. The OD value of each well was measured at 450 nm using a microplate reader.

C11-BODIPY staining for lipid peroxidation. OS cells were washed with PBS and incubated with 2 μM C11-BODIPY 581/591 probe (Thermo Fisher Scientific, Inc.) at 37˚C for 30 min in the dark. After washing with PBS, the cells were observed under a fluorescence microscope. Images of green fluorescence (oxidized BODIPY) and red fluorescence (reduced BODIPY) were captured, and the green/red fluorescence intensity ratio was determined using ImageJ software (version 1.54).

Table I. Primer and siRNA sequences used in the present study.

Name	Sequence, 5'-3'
GAPDH-F	GAGTCAACGGATTTGGTCGT
GAPDH-R	TTGATTTTGGAGGGATCTCG
SLC7A11-F	GGCAGTGACCTTTTCTGAGC
SLC7A11-R	TCATTGTCAAAGGGTGCAAA
KIAA1429-F	CTCGGCGATGGAGCTGTTAT
KIAA1429-R	CTCGGCGATGGAGCTGTTAT
si-NC-F	UUCUCCGAACGUGUCACGUTT
si-NC-R	ACGUGACACGUUCGGAGAATT
si-KIAA1429-1-S	AGUAUCUAAAAAUAACAGCUC
si-KIAA1429-1-AS	GCUGUUAUUUUUAGAUACUUU
si-KIAA1429-2-S	AAGUAUCUAAAAAUAACAGCU
si-KIAA1429-2-AS	CUGUUAUUUUUAGAUACUUUU
si-KIAA1429-3-S	AGUCUAAUUGAAAUGUAUGGG
si-KIAA1429-3-AS	CAUACAUUUCAAUUAGACUUA

AS, antisense; F, forward; NC, negative control; R, reverse; S, sense; si, small interfering; SLC7A11, solute carrier family 7 member 11.

m6A-modified RNA immunoprecipitation (MeRIP). The m6A modification levels of KIAA1429-targeted mRNAs were detected by MeRIP-qPCR assay using a Magna MeRIP m6A kit (cat no. 17-10499; Sigma-Aldrich; Merck KGaA) (19), according to the manufacturer's instructions. Total RNA was extracted from 143B and U2OS cells as aforementioned, with a yield greater than 300 μg; one-tenth of the total RNA (~30 μg) was used as the input control. The remaining RNA was subjected to immunoprecipitation. For immunoprecipitation, the RNA was incubated overnight at 4˚C with 2 μg anti-m6A antibody (cat. no. ABE572) or 2 μg normal rabbit IgG (cat. no. 12-370) (both from MilliporeSigma) as a negative control in a total volume of 500 μl immunoprecipitation buffer overnight at 4˚C with gentle rotation. Thereafter, 20 μl Protein A/G magnetic beads (MilliporeSigma) were added to each sample and the mixture was incubated for an additional 2 h at 4˚C with rotation. The beads were then collected using a magnetic stand and washed three times with 500 μl immunoprecipitation buffer. The captured RNA was eluted by adding 150 μl elution buffer (10 mM Tris-HCl, pH 7.4; 1 mM EDTA; 0.5% SDS) and incubating at 65˚C for 10 min with gentle shaking. The eluted RNA was then purified using spin columns. The purified RNA was analyzed by RT-qPCR as aforementioned and relative m6A enrichment was normalized to the IgG control group.

Dual-luciferase reporter assay. The wild-type (WT) and mutant (MUT) 3'UTR sequences of SLC7A11 were synthesized and cloned into the pmirGLO dual-luciferase reporter vector (cat. no. E1330; Promega Corporation). This vector contains both firefly luciferase (reporter) and *Renilla*

luciferase (internal control) genes. The recombinant plasmids (Luc-SLC7A11-3'UTR-WT and Luc-SLC7A11-3'UTR-MUT) were prepared using standard molecular cloning techniques (20). For the reporter assay, 143B and U2OS cells were seeded in 24-well plates at 70-80% confluence and co-transfected with 100 ng WT or MUT reporter plasmid, 50 nM si-NC or si-KIAA1429 (si-KIAA1429-1 or si-KIAA1429-2) and 5 ng *Renilla* luciferase control plasmid (pRL-TK; Promega Corporation) using Lipofectamine 3000 according to the manufacturer's instructions. After 36 h of transfection at 37˚C, the cells were lysed and centrifuged at 12,000 x g for 1 min, and luciferase activity was measured using a Dual-Luciferase Reporter Assay System (cat. no. E1910; Promega Corporation). Firefly luciferase activity was normalized to *Renilla* luciferase activity for each well. The relative luciferase activity was calculated as the ratio of normalized firefly luciferase activity in the si-KIAA1429-transfected groups to that in the si-NC group.

Subcutaneous xenograft tumor model in nude mice. All animal procedures were approved by the Animal Ethics Committee of Ganzhou People's Hospital (approval no. PJD2026-025-01; Ganzhou, China) and conducted in accordance with institutional guidelines. Male BALB/c nude mice (age, 6-8 weeks; weight, 18-20 g) were purchased from SPF (Beijing) Biotechnology Co. Ltd. All animals were housed in individually ventilated cages under specific pathogen-free conditions. The animal room was maintained at an ambient temperature of 22±2˚C with a relative humidity of 50±5% and a 12/12-h light/dark cycle. Mice had *ad libitum* access to sterilized standard rodent chow and autoclaved water. The mice were randomly divided into the following three groups (n=6/each group): Short hairpin (sh)RNA NC lentivirus (lv-sh-NC) group, lentivirus carrying shRNA targeting KIAA1429 (lv-sh-KIAA1429) group and lv-sh-KIAA1429 + lentivirus encoding SLC7A11 (lv-SLC7A11) group.

Second-generation lentiviral particles were produced by co-transfection of 293T cells (Lenti-X™ 293T Cell Line; cat. no. 632180; Takara Bio, Inc.) with a transfer vector, a packaging plasmid (psPAX2; cat. no. 12260; Addgene, Inc.) and an envelope plasmid (pMD2.G; cat. no. 12259; Addgene, Inc.). For KIAA1429 knockdown, the transfer vector was pLKO.1 (cat. no. 8453; Addgene, Inc.) containing sh-KIAA1429. Notably, lv-sh-NC was generated using a scramble shRNA control vector (cat. no. 1864; Addgene, Inc.), which contained a scrambled, non-targeting shRNA sequence in the pLKO.1 backbone. For SLC7A11 overexpression, the transfer vector was a lentiviral vector (pCDH-EF1α-MCS-T2A-Puro) containing the full-length human SLC7A11 cDNA. The coding sequence of SLC7A11 in this lentiviral vector was identical to that of the pcDNA3.1-based oe-SLC7A11 plasmid used in the *in vitro* experiments. For lentivirus production, 293T cells were seeded at $5x10^6$ cells/10-cm dish and cultured overnight to reach 70-80% confluence. The transfection mixture (12 μg transfer vector, 6 μg psPAX2 packaging plasmid and 3 μg pMD2.G envelope plasmid) was incubated with the cells for 6-8 h at 37˚C, after which the medium was replaced with fresh DMEM containing 10% FBS. Viral supernatant was collected at 48 and 72 h post-transfection, pooled and clarified by centrifugation at 3,000 x g for 10 min at 4˚C, followed by filtration through a 0.45-μm sterile filter (Sigma-Aldrich; Merck KGaA). The clarified supernatant was then concentrated by ultracentrifugation at 50,000 x g for 2 h at 4˚C using a Beckman SW-32 Ti rotor (Beckman Coulter, Inc.). The viral pellet was then resuspended in PBS, aliquoted and stored at -80˚C until use. Viral titers were determined by RT-qPCR.

For transduction, the culture medium of U2OS cells was replaced with fresh DMEM containing 8 μg/ml polybrene (cat. no. TR-1003; Sigma-Aldrich; Merck KGaA). Lentiviral supernatant (lv-sh-NC, lv-sh-KIAA1429, lv-NC or lv-SLC7A11) was added at a multiplicity of infection of 10. The cells were incubated with the virus for 24 h at 37˚C in a 5% CO_2 incubator. After 24 h, the virus-containing medium was removed and replaced with fresh complete DMEM. Transduced cells were selected with puromycin (2 μg/ml; InvivoGen) for 7 days. Puromycin-resistant cells were expanded and maintained in complete medium containing 1 μg/ml puromycin. A total of $2x10^6$ U2OS cells in 100 μl PBS were subcutaneously injected into the right flank of each mouse Tumor growth and body weight were monitored weekly, and tumor volume was calculated using the formula $V=(L \times W^2)/2$, where L is the longest diameter and W is the shortest diameter. The maximum tumor volume recorded during the 28-day study was 889.35 mm^3 and the maximum tumor diameter was 14.7 mm, both within the limits approved by the Animal Ethics Committee of Ganzhou People's Hospital. After 28 days, the mice were placed in an induction chamber containing 4% isoflurane in 100% oxygen at a flow rate of 1 l/min. After successful induction of anesthesia, the mice were maintained under 1.5% isoflurane anesthesia delivered via a nose cone until deep anesthesia was confirmed, immediately followed by cervical dislocation for euthanasia. The tumors were then excised and weighed, and images were captured. Humane endpoints were pre-established as follows: Tumor volume >2,000 mm^3, tumor diameter >20 mm, tumor ulceration, severe weight loss (>20% of initial body weight) or signs of severe pain/distress. No mice reached these endpoints during the 28-day observation period, and all animals were euthanized at the scheduled endpoint.

Hematoxylin and eosin (H&E) staining. Tumor tissues were fixed in 4% paraformaldehyde at 4˚C for 24 h and dehydrated through graded ethanol solutions. After xylene clearing, the samples were embedded in paraffin, and the sections (4 μm) were prepared, mounted on glass slides and air-dried. For staining, the sections were deparaffinized in xylene (two changes, 10 min each at room temperature), rehydrated through a descending ethanol series at room temperature, stained with hematoxylin (3-5 min) at room temperature, differentiated in 1% acid alcohol and rinsed under tap water for bluing at room temperature. Sections were then counterstained with eosin (40-60 sec), dehydrated, cleared in xylene and mounted with neutral balsam at room temperature. Images were acquired using a bright-field microscope.

Immunohistochemistry (IHC). Following deparaffinization and rehydration, 4-µm paraffin-embedded tissue sections, prepared as aforementioned, underwent microwave-assisted antigen retrieval in citrate buffer (10 mM, pH 6.0) for 15 min at 95˚C. Endogenous peroxidase activity was blocked by incubation with 0.3% H_2O_2 in PBS for 30 min at room temperature,

and the sections were then washed three times with PBS and blocked with 3% BSA in PBS for 1 h at room temperature. Subsequently, the tissues were incubated overnight at 4˚C with a primary anti-Ki67 antibody (1:400; cat. no. ab15580; Abcam). After washing, the slides were incubated with a HRP-conjugated goat anti-rabbit secondary antibody (1:200; cat. no. ab6721; Abcam) for 80 min at room temperature. The signals were developed using a diaminobenzidine substrate (Sigma-Aldrich; Merck KGaA) for 2-5 min at room temperature and nuclei were counterstained with hematoxylin (Sigma-Aldrich; Merck KGaA) for 1 min at room temperature. Slides were subsequently dehydrated, cleared and mounted, with staining visualized under a light microscope.

Western blot analysis. The protein expression levels of KIAA1429, cytochrome *c* oxidase 2 (COX2), GPX4, SLC7A11, E-cadherin and Vimentin were determined by western blotting. Total protein was extracted from cells and excised xenograft tumor tissues using RIPA lysis buffer [50 mM Tris-HCl (pH 7.4), 150 mM NaCl, 1% NP-40, 0.5% sodium deoxycholate, 0.1% SDS, supplemented with protease and phosphatase inhibitors; Beyotime Biotechnology], and protein concentrations were measured using a Pierce BCA Protein Assay Kit (Thermo Fisher Scientific, Inc.). Proteins (20 μg/lane) were separated by electrophoresis on a 10% sodium dodecyl sulfate-polyacrylamide gel and subsequently transferred onto polyvinylidene fluoride membranes. After blocking with 5% skim milk in Tris-buffered saline containing 0.1% Tween-20for 1 h at room temperature, the membranes were incubated overnight at 4˚C with the following primary antibodies (all 1:1,000; Abcam): Anti-KIAA1429 (cat. no. ab271136), anti-COX2 (cat. no. ab179800), anti-GPX4 (cat. no. ab125066), anti-SLC7A11 (cat. no. ab307601), anti-E-cadherin (cat. no. ab40772), anti-Vimentin (cat. no. ab92547) and anti-GAPDH (cat. no. ab9485). The membranes were then incubated with goat anti-rabbit horseradish peroxidase (HRP)-conjugated secondary antibodies (1:5,000; cat. no. ab6721; Abcam) at room temperature for 1 h. Protein bands were visualized using SuperSignal™ West Pico PLUS Chemiluminescent Substrate (Thermo Fisher Scientific, Inc.) and imaged with a Tanon 5200 chemiluminescent imaging system (Tanon Science and Technology Co., Ltd.). Semi-quantification of band intensities was performed using ImageJ software (version 1.54).

Statistical analysis. All statistical analyses were performed using GraphPad Prism 8.0 (Dotmatics) and the data are presented as the mean ± standard deviation. All *in vitro* experiments were independently performed at least three times. Differences between two groups were analyzed using unpaired Student's t-test. For multiple group comparisons, one-way analysis of variance was used, followed by Tukey's honestly significant difference test for post hoc pairwise comparisons. $P<0.05$ was considered to indicate a statistically significant difference.

Results

Downregulation of KIAA1429 suppresses proliferation, invasion and migration in OS Cells. Western blot analysis was performed to determine KIAA1429 expression levels (Fig. 1A), revealing a marked increase in all OS cell lines (MG63, 143B, U2OS, and Saos-2) compared with in normal human osteoblastic cells (hFOB1.19). Among the OS cell lines tested, 143B and U2OS cells showed relatively high KIAA1429 expression, and were selected for subsequent functional assays because of their high transfection efficiency. To investigate the functional role of KIAA1429, 143B and U2OS cells were transfected with three independent siRNAs targeting KIAA1429, along with si-NC and untreated groups. Western blot analysis confirmed a significant reduction in KIAA1429 protein levels in the siRNA-transfected groups compared with those in the si-NC group (Fig. 1B), indicating efficient knockdown. Cell proliferation was assessed using CCK-8 assays in 143B and U2OS cells transfected with si-NC, si-KIAA1429-1 or si-KIAA1429-2; KIAA1429 knockdown significantly inhibited cell proliferation compared with in the si-NC group (Fig. 1C). Furthermore, apoptosis was evaluated by flow cytometry, which showed a significant increase in apoptosis rates in both the si-KIAA1429-1 and si-KIAA1429-2 groups relative to si-NC-transfected cells (Fig. 1D). Cell invasion and migration were assessed using Transwell and wound healing assays, respectively, demonstrating that both the invasive and migratory abilities of OS cells were markedly impaired following KIAA1429 knockdown (Fig. 2A and B). Collectively, these results indicated that downregulation of KIAA1429 may suppress proliferation, invasion and migration, while promoting apoptosis in OS cells.

Downregulation of KIAA1429 promotes ferroptosis in OS cells. To investigate whether KIAA1429 modulates ferroptosis, 143B and U2OS cells transfected with si-NC and si-KIAA1429 were treated with the ferroptosis inducer erastin. CCK-8 assays showed that cell viability was significantly reduced in the si-NC + erastin group compared with in the si-NC group (Fig. 3A). Moreover, KIAA1429 knockdown further decreased cell viability in both the si-KIAA1429-1 + erastin and si-KIAA1429-2 + erastin groups compared with in the si-NC + erastin group. Western blot analysis of ferroptosis-related proteins revealed that erastin treatment alone (si-NC + erastin) significantly increased COX2 expression and decreased GPX4 expression compared with in the si-NC group (Fig. 3B). Notably, KIAA1429 knockdown synergized with erastin to further enhance COX2 expression and suppress GPX4 levels. ELISA was performed to measure oxidative stress (MDA and GSH) and ferroptosis-related markers (Fe^{2+} and ROS) levels. Erastin treatment significantly increased MDA, iron and ROS levels, while reducing GSH concentrations compared with in the si-NC group (Fig. 3C). KIAA1429 knockdown further intensified these effects, resulting in more pronounced alterations in these ferroptosis-related markers. Lipid peroxidation was further assessed using C11-BODIPY staining. Erastin treatment markedly increased the green/red fluorescence ratio compared with that in the si-NC group, indicating elevated lipid peroxidation in 143B and U2OS cells (Fig. 3D). KIAA1429 knockdown further enhanced this effect, as shown by significantly higher green/red fluorescence ratios in both the erastin + si-KIAA1429-1 and erastin + si-KIAA1429-2 groups compared with in the si-NC + erastin group. Collectively, these results indicated that KIAA1429 downregulation enhances erastin-induced ferroptosis in OS cells.

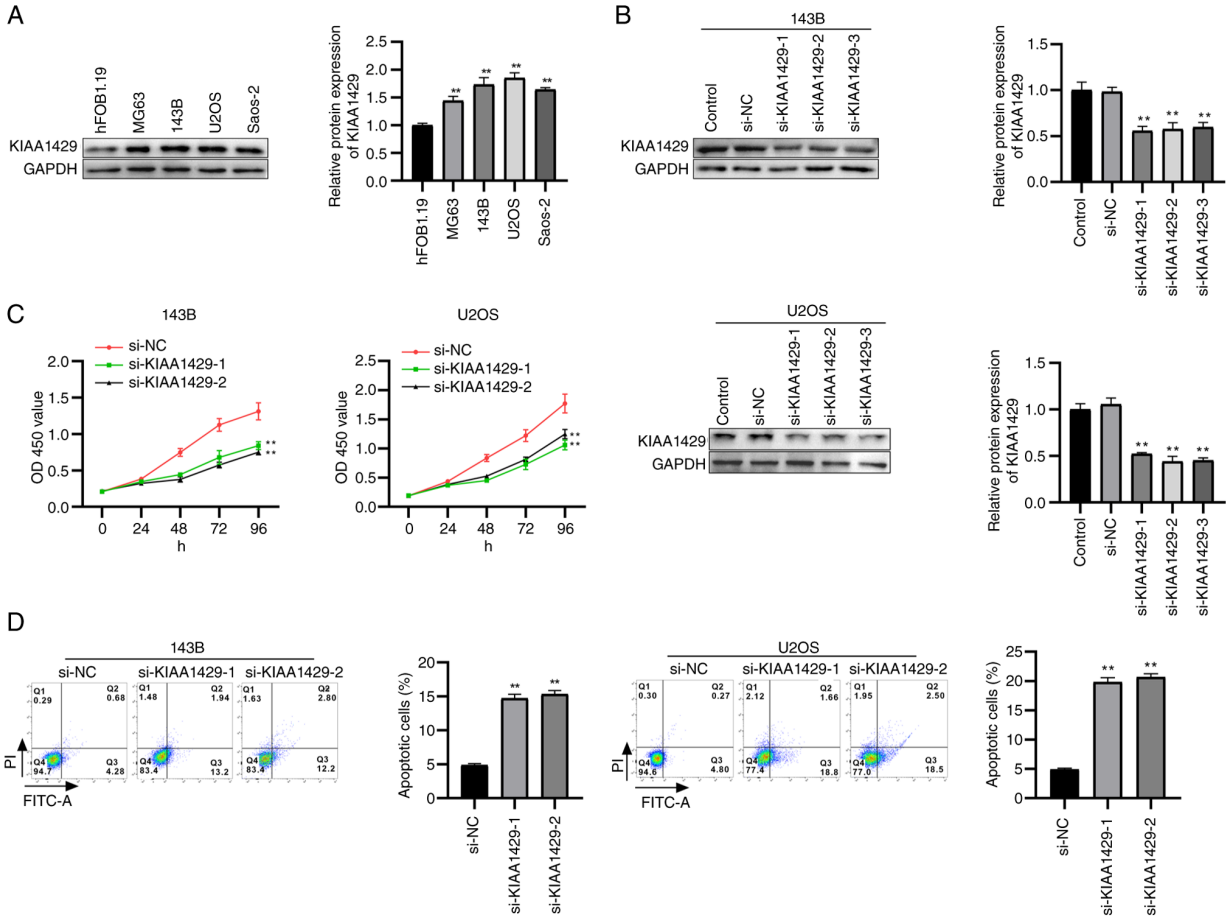

Figure 1. KIAA1429 knockdown suppresses OS cell proliferation and promotes apoptosis. (A) KIAA1429 expression in OS cell lines was detected by western blotting. **P<0.01 vs. hFOB 1.19 group. (B) KIAA1429 knockdown efficiency was measured by western blotting. (C) Cell proliferation was assessed by Cell Counting Kit-8 assay. (D) Apoptosis detection via flow cytometry. **P<0.01 vs. si-NC group. NC, negative control; OD, optical density; OS, osteosarcoma; PI, propidium iodide; si, small interfering.

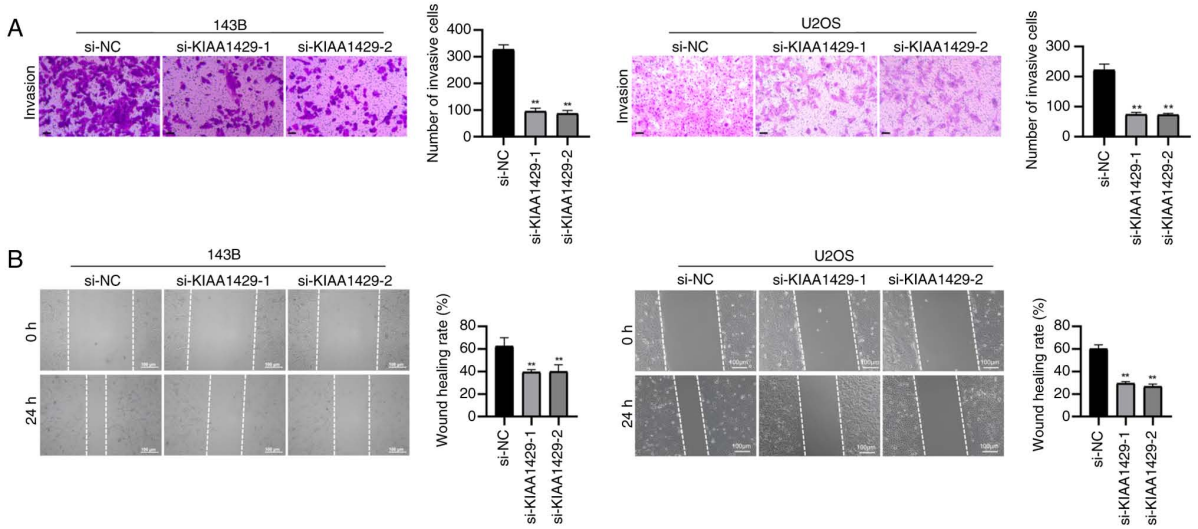

Figure 2. KIAA1429 knockdown suppresses osteosarcoma cell invasion and migration. (A) Cell invasion was measured by Transwell assay (magnification, x200; scale bar, 100 μm). (B) Cell migration was evaluated by wound healing assay (magnification, x200; scale bar, 100 μm). **P<0.01 vs. si-NC group. NC, negative control; si, small interfering.

Downregulation of KIAA1429 inhibits SLC7A11 expression via m6A modification. Given that KIAA1429 has been reported to bind to m6A sites on the SLC7A11 transcript and affect the progression of hepatocellular carcinoma (21), the current study aimed to elucidate its role in OS. Western blot analysis confirmed that SLC7A11 expression was significantly higher

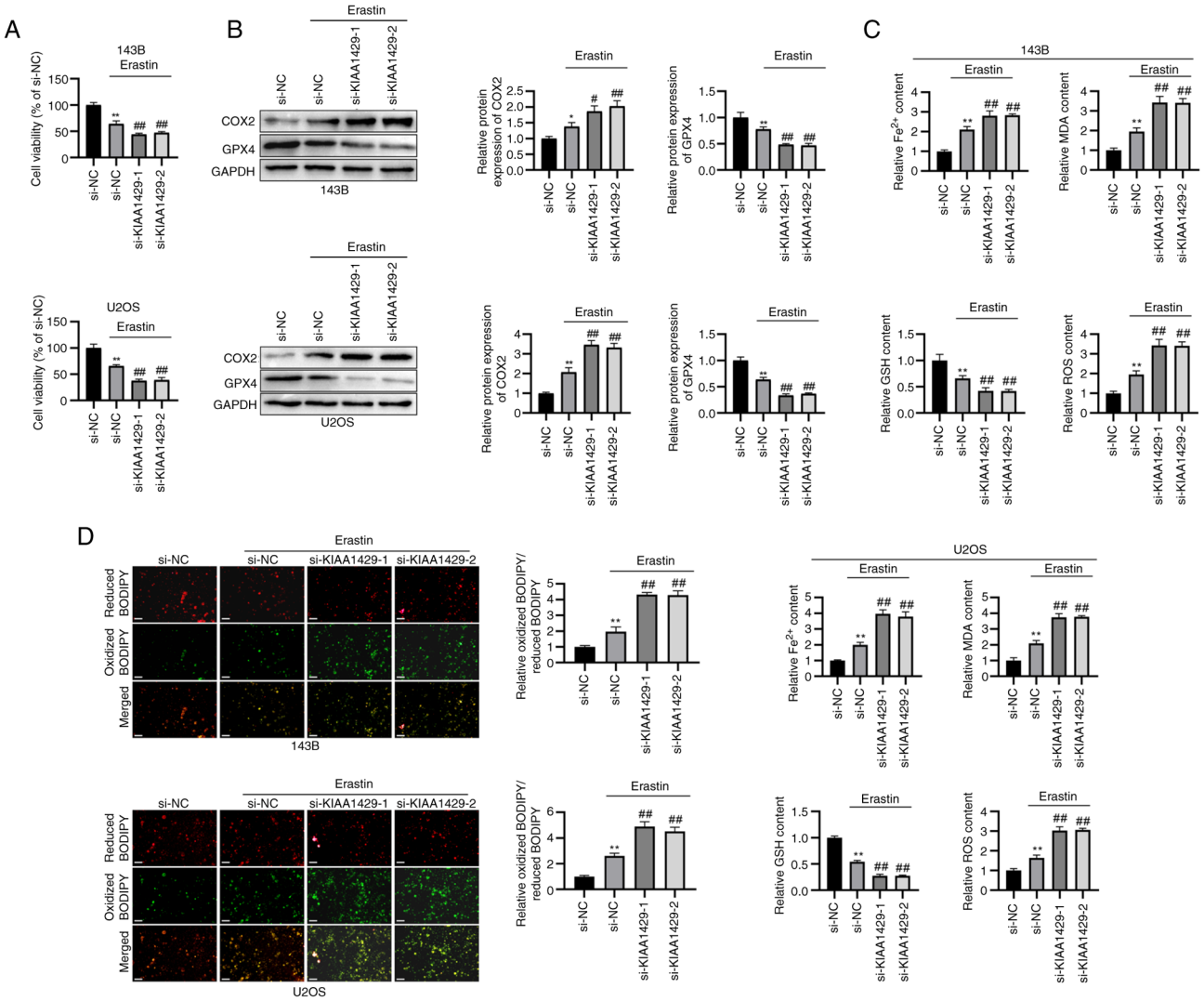

Figure 3. KIAA1429 knockdown promotes ferroptosis in osteosarcoma cells. (A) Cell viability was evaluated by Cell Counting Kit-8 assay. (B) Protein expression levels of ferroptosis-related markers were measured by western blotting. (C) ELISA was performed to evaluate levels of MDA, Fe^{2+}, GSH and ROS. (D) C11-BODIPY staining for lipid peroxidation (magnification, x200; scale bar, 100 μm). *P<0.05, **P<0.01 vs. si-NC; $^{\#}$P<0.05, $^{\#\#}$P<0.01 vs. si-NC group. COX2, cytochrome *c* oxidase 2; GPX4, GSH peroxidase 4; GSH, glutathione; MDA, malondialdehyde; NC, negative control; ROS, reactive oxygen species; si, small interfering.

in human OS cell lines (MG63, 143B, U2OS and Saos-2) than in the normal osteoblastic cell line hFOB1.19 (Fig. 4A). Both RT-qPCR and western blot analysis showed that KIAA1429 knockdown significantly reduced SLC7A11 expression at both the mRNA and protein levels compared with in the si-NC group (Fig. 4B and C). MeRIP-qPCR assays further demonstrated that m6A enrichment of SLC7A11 mRNA was markedly decreased following KIAA1429 knockdown (Fig. 4D). To assess mRNA stability, cells were treated with actinomycin D (5 μg/ml) and qPCR was performed at different time points. The results showed that SLC7A11 mRNA decayed more rapidly in KIAA1429-knockdown cells than in control cells (Fig. 4E). Using a dual-luciferase reporter assay, it was revealed that KIAA1429 knockdown significantly reduced luciferase activity of SLC7A11-WT, whereas no significant effect was observed on SLC7A11-MUT (Fig. 4F). Collectively, these findings indicated that KIAA1429 knockdown could suppress SLC7A11 expression through an m6A-dependent mechanism, thereby reducing mRNA stability and translational regulation.

KIAA1429 knockdown alleviates OS progression by regulating SLC7A11 expression. To investigate the functional role of KIAA1429 and its interaction with SLC7A11 in OS, SLC7A11 was overexpressed in 143B and U2OS cells. RT-qPCR analysis was performed to evaluate the expression of SLC7A11 in 143B and U2OS cells, confirming the successful overexpression of SLC7A11 in cells transfected with oe-SLC7A11 (Fig. 5A). CCK-8 assays showed that KIAA1429 knockdown significantly inhibited cell proliferation compared with that in the si-NC group (Fig. 5B). By contrast, SLC7A11 overexpression partially rescued this inhibitory effect in the rescue group (si-KIAA1429 + oe-SLC7A11). Flow cytometric analysis demonstrated that KIAA1429 knockdown significantly increased apoptosis compared with in the si-NC group, whereas SLC7A11 overexpression partially reversed this pro-apoptotic effect (Fig. 5C). Transwell and wound healing assays revealed that KIAA1429 silencing markedly reduced the invasive and migratory abilities of OS cells compared with in the si-NC group; however, these effects were significantly attenuated

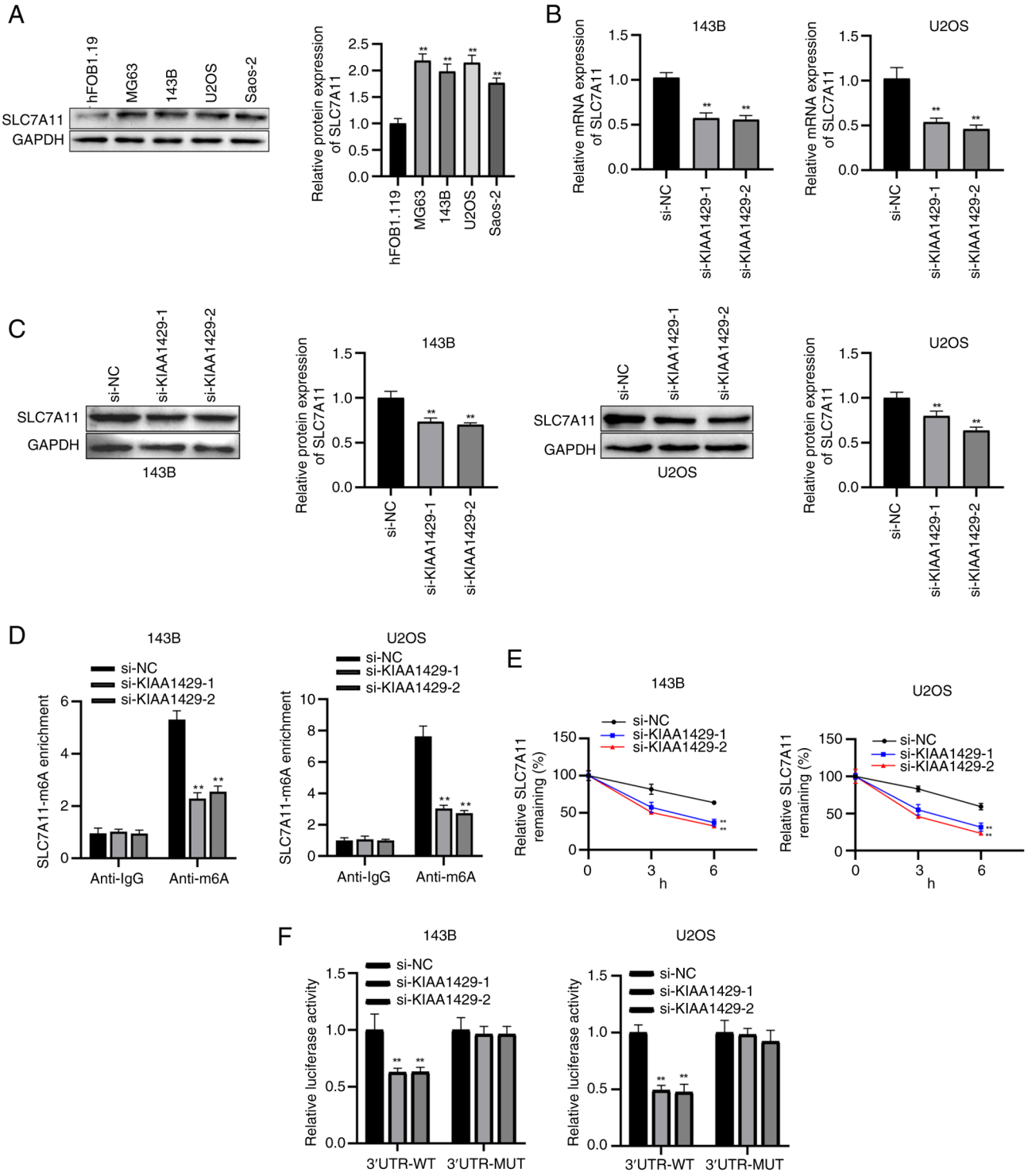

Figure 4. Mechanistic regulation of SLC7A11 by KIAA1429 through m6A modification. (A) SLC7A11 expression in osteosarcoma cell lines was detected by western blotting. **P<0.01 vs. hFOB1.19. (B) mRNA and (C) protein levels of SLC7A11 in transfected 143B and U2OS cells were measured by reverse transcription-qPCR and western blotting, respectively. (D) m6A enrichment of SLC7A11 was measured by m6A-modified RNA immunoprecipitation-qPCR. (E) Stability of SLC7A11 after actinomycin treatment was detected by qPCR. (F) Dual luciferase assay was used to verify the interaction between KIAA1429 and SLC7A11. **P<0.01 vs. si-NC. m6A, N6-methyladenosine; MUT, mutant; NC, negative control; qPCR, quantitative PCR; si, small interfering; SLC7A11, solute carrier family 7 member 11; WT, wild-type.

by SLC7A11 overexpression (Fig. 6A and B). Furthermore, western blot analysis of epithelial-mesenchymal transition (EMT)-related proteins showed that, compared with in the si-NC group, the si-KIAA1429 group exhibited increased E-cadherin expression and decreased Vimentin expression (Fig. 6C). Notably, SLC7A11 overexpression partially reversed these changes, resulting in decreased E-cadherin and increased Vimentin levels compared with in the si-KIAA1429 group (Fig. 6C). Thus, KIAA1429 knockdown may suppress EMT, and this effect was partially dependent on SLC7A11 downregulation. Collectively, these findings indicated that KIAA1429 may promote OS cell proliferation, invasion

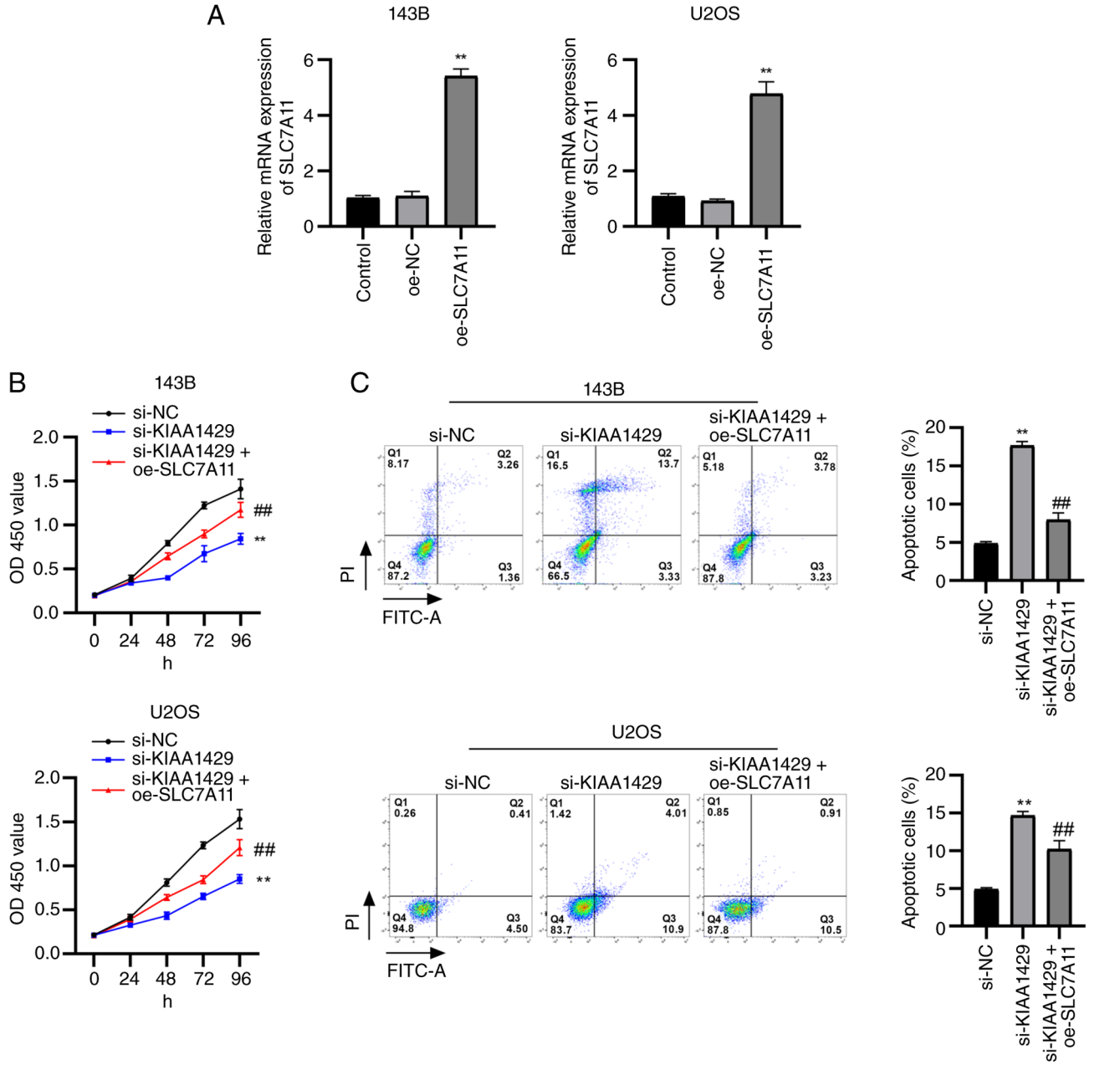

Figure 5. KIAA1429 knockdown suppresses viability and promotes apoptosis in OS cells via SLC7A11. (A) Reverse transcription-quantitative PCR was performed to detect the mRNA levels of SLC7A11 in OS cell lines. **P<0.01 vs. oe-NC. (B) Cell viability was measured by Cell Counting Kit-8 assay. (C) Apoptosis was evaluated by flow cytometry. **P<0.01 vs. si-NC; $^{\#\#}$P<0.01 vs. si-KIAA1429. NC, negative control; OD, optical density; oe, overexpression vector; OS, osteosarcoma; si, small interfering; SLC7A11, solute carrier family 7 member 11.

and migration while inhibiting apoptosis, largely through regulation of SLC7A11 expression.

KIAA1429 modulates ferroptosis in OS via regulation of SLC7A11. CCK-8 assays showed that erastin treatment significantly reduced cell viability in the si-NC + erastin group compared with in the si-NC group (Fig. 7A). KIAA1429 knockdown further enhanced erastin-induced cytotoxicity, resulting in an additional decrease in cell viability; however, SLC7A11 overexpression partially reversed the reduction in cell viability caused by KIAA1429 knockdown (Fig. 7A). ELISA was used to detect the levels of ferroptosis-related markers and showed that erastin treatment increased MDA, Fe^{2+} and ROS levels, while decreasing GSH concentrations; these effects were further enhanced by KIAA1429 knockdown but were significantly attenuated by SLC7A11 overexpression (Fig. 7B). Western blot analysis of ferroptosis-related proteins revealed that erastin treatment upregulated COX2 and downregulated GPX4 compared with in the si-NC group, and KIAA1429 silencing further amplified these effects; however, simultaneous overexpression of SLC7A11 counteracted the effects of KIAA1429 knockdown, leading to decreased COX2 and increased GPX4 expression (Fig. 7C). The expression of EMT-related markers was also evaluated under ferroptosis-inducing conditions. Western blot analysis showed that erastin treatment alone increased E-cadherin and decreased Vimentin levels compared with those in the si-NC group, and KIAA1429 knockdown (erastin + si-KIAA1429 group) further enhanced

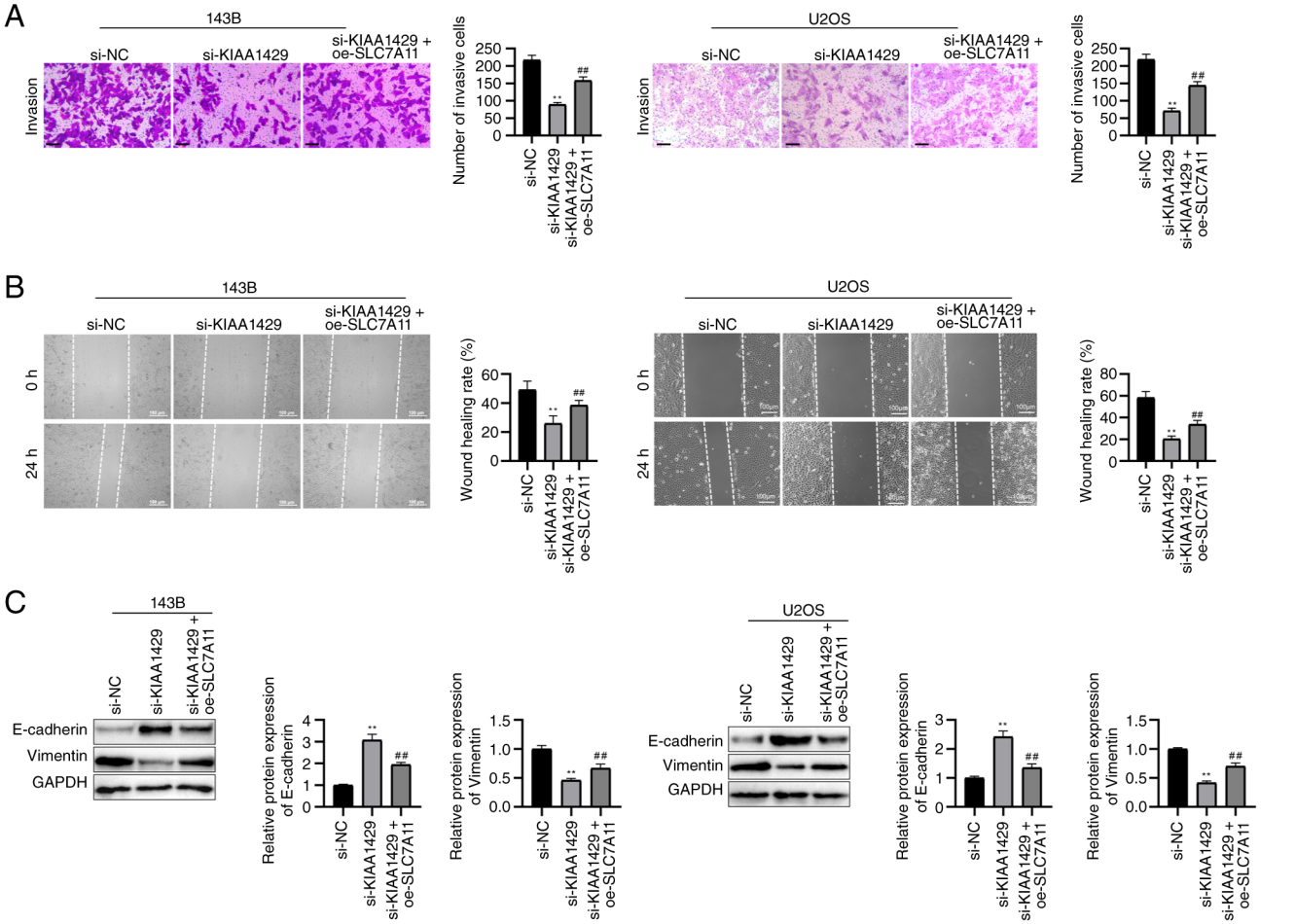

Figure 6. KIAA1429 knockdown suppresses invasion, migration and epithelial-mesenchymal transition in OS cells via SLC7A11. (A) Invasive potential was measured by Transwell assay (magnification, x200; scale bar, 100 μm). (B) Migratory capacity was evaluated by wound healing assay (magnification, x200; scale bar, 100 μm). (C) Western blot analysis of E-cadherin and Vimentin expression. **P<0.01 vs. si-NC; $^{\#\#}$P<0.01 vs. si-KIAA1429. NC, negative control; OD, optical density; oe, overexpression vector; OS, osteosarcoma; si, small interfering; SLC7A11, solute carrier family 7 member 11.

these changes (Fig. 7D). However, SLC7A11 overexpression (erastin + si-KIAA1429 + oe-SLC7A11) significantly reversed these effects, as evidenced by decreased E-cadherin and increased Vimentin expression levels (Fig. 7D). Collectively, these results demonstrated that KIAA1429 knockdown could sensitize OS cells to erastin-induced ferroptosis and suppress EMT, likely through downregulation of SLC7A11, whereas SLC7A11 overexpression mitigates this effect.

KIAA1429 knockdown suppresses OS growth and ferroptosis in vivo. To evaluate the role of KIAA1429 in OS progression and ferroptosis *in vivo*, BALB/c nude mice were subcutaneously injected with U2OS cells stably transduced with lentiviral constructs. Successful overexpression of SLC7A11 by lv-SLC7A11 was confirmed in U2OS cells prior to injection into mice (Fig. S1). Compared with in the lv-sh-NC group, KIAA1429 expression was significantly reduced in the tumor tissues of the lv-sh-KIAA1429 group, indicating successful knockdown of KIAA1429 *in vivo*; no significant difference in KIAA1429 expression was observed between the lv-sh-KIAA1429 and lv-sh-KIAA1429 + lv-SLC7A11 groups (Fig. 8A). Tumors were excised at the endpoint (Fig. 8B), and tumor weight and volume were measured. Compared with in the lv-sh-NC group, tumors in the lv-sh-KIAA1429 group exhibited significantly reduced weight and volume (Fig. 8C). By contrast, SLC7A11 overexpression partially restored tumor growth compared with in the lv-sh-KIAA1429 group.

H&E staining of tumor tissues revealed that the lv-sh-NC group exhibited densely arranged tumor cells with minimal inflammatory infiltration (Fig. 8D). By contrast, the lv-sh-KIAA1429 group exhibited a disrupted tissue architecture with pronounced inflammatory infiltration. The lv-sh-KIAA1429 + lv-SLC7A11 group displayed partially restored cellular density and reduced inflammatory infiltration compared with the lv-sh-KIAA1429 group. IHC analysis of Ki67 expression showed a marked reduction in Ki67-positive cells in the lv-sh-KIAA1429 group compared with in the lv-sh-NC group, whereas this effect was partially reversed by SLC7A11 overexpression (Fig. 8E). ELISA of ferroptosis-related markers showed that KIAA1429 knockdown increased MDA, iron and ROS levels, while decreasing GSH concentrations compared with in the lv-sh-NC group; however, these changes were attenuated by SLC7A11 overexpression (Fig. 8F). Western blot analysis further demonstrated that KIAA1429 knockdown increased COX2 expression and decreased SLC7A11 expression, whereas SLC7A11 overexpression partially reversed these

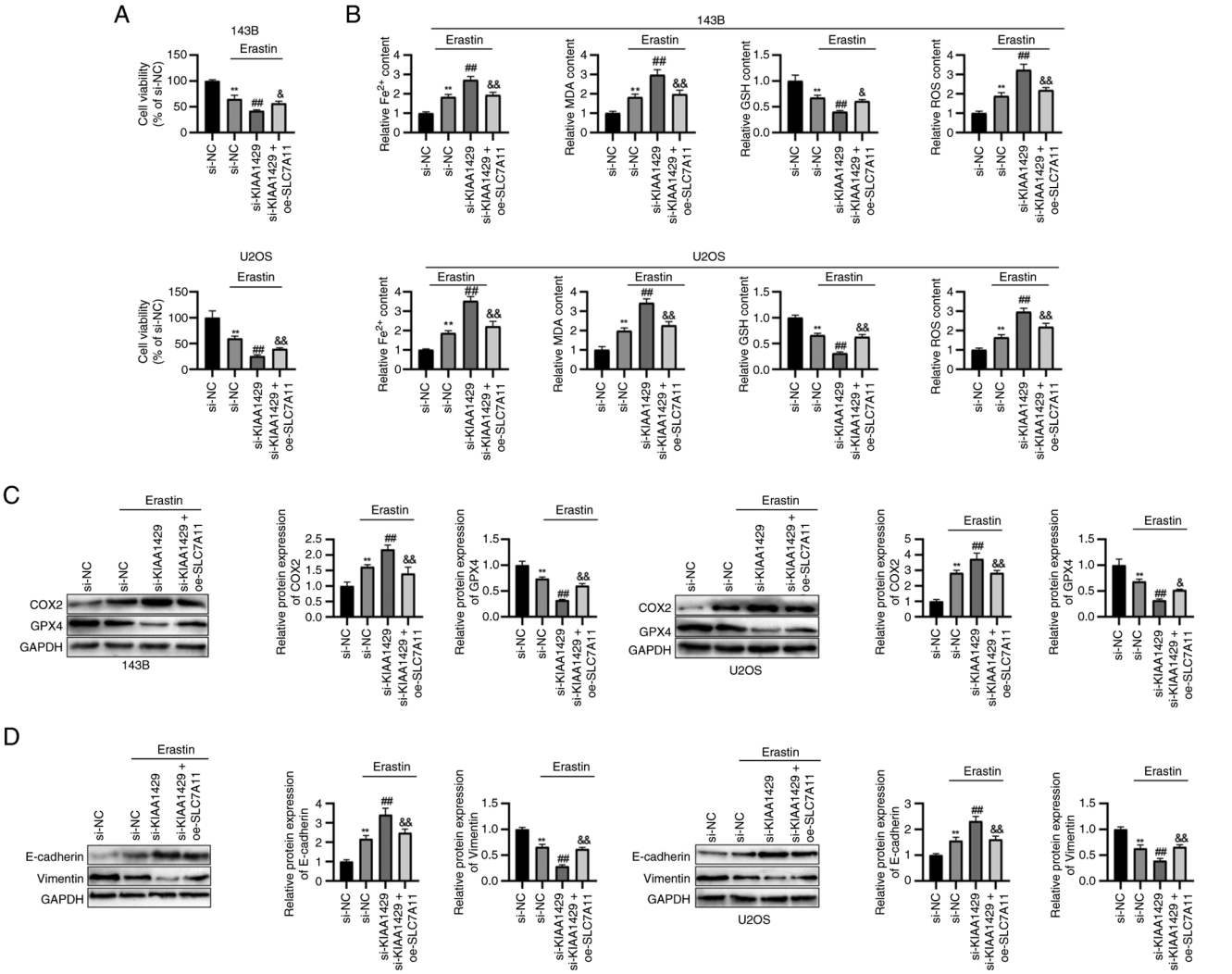

Figure 7. KIAA1429/SLC7A11 axis regulates ferroptosis in osteosarcoma. (A) Cell viability was assessed by Cell Counting Kit-8 assay. (B) Levels of oxidative stress parameters (Fe^{2+}, MDA, GSH, and ROS) were assessed by ELISA. (C) Ferroptosis markers (COX2 and GPX4) were measured by western blotting. (D) Western blot analysis of E-cadherin and Vimentin expression. **P<0.01 vs. si-NC; $^{\#\#}$P<0.01 vs. si-NC + erastin; $^{\&}$P<0.05, $^{\&\&}$P<0.01 vs. si-KIAA1429 + erastin. COX2, cytochrome *c* oxidase 2; GPX4, GSH peroxidase 4; GSH, glutathione; MDA, malondialdehyde; NC, negative control; oe, overexpression vector; ROS, reactive oxygen species; si, small interfering; SLC7A11, solute carrier family 7 member 11.

effects (Fig. 8G). Collectively, these *in vivo* findings confirmed that KIAA1429 downregulation may suppress tumor growth and enhance ferroptosis in OS, largely through regulation of SLC7A11.

Discussion

OS poses severe clinical risks, including debilitating pain, pathological fractures, limb dysfunction and frequent pulmonary metastasis, which collectively account for its high mortality rate (22,23). The present study demonstrated that KIAA1429 was highly expressed in OS cell lines, and that its knockdown markedly suppressed malignant tumor progression. Mechanistically, KIAA1429 stabilized SLC7A11 mRNA via m6A methylation, thereby inhibiting ferroptosis and facilitating tumor progression. These findings indicated that KIAA1429 may be a critical oncogenic driver in OS.

As the predominant internal modification within eukaryotic mRNAs, m6A orchestrates gene expression dynamics through its cognate 'writer', 'eraser' and 'reader' protein machinery, exerting regulatory control over RNA splicing, stability, translation efficiency and decay pathways (24). Its dysregulation is increasingly implicated in the oncogenesis of various types of cancer (25). In OS, m6A methylation affects tumor invasion and metastasis through various signaling pathways (26). As an m6A methyltransferase, methyltransferase-like 3 drives OS cell progression through dual mechanisms: Regulating the m6A modification status of lymphoid enhancer-binding factor 1 and activating the Wnt/β-catenin signaling cascade (27). The demethylase AlkB homologue 5 facilitates tumor growth and metastasis by erasing m6A marks on targets such as ubiquitin-specific peptidase 22, thereby disrupting histone ubiquitination and enhancing DNA replication and repair processes (28). By revealing the critical contribution of m6A to OS initiation and progression, these findings simultaneously position it as a viable therapeutic target.

The m6A methyltransferase complex harbors KIAA1429, a critical regulatory component involved in the pathogenesis of numerous types of human cancer. In hepatocellular carcinoma,

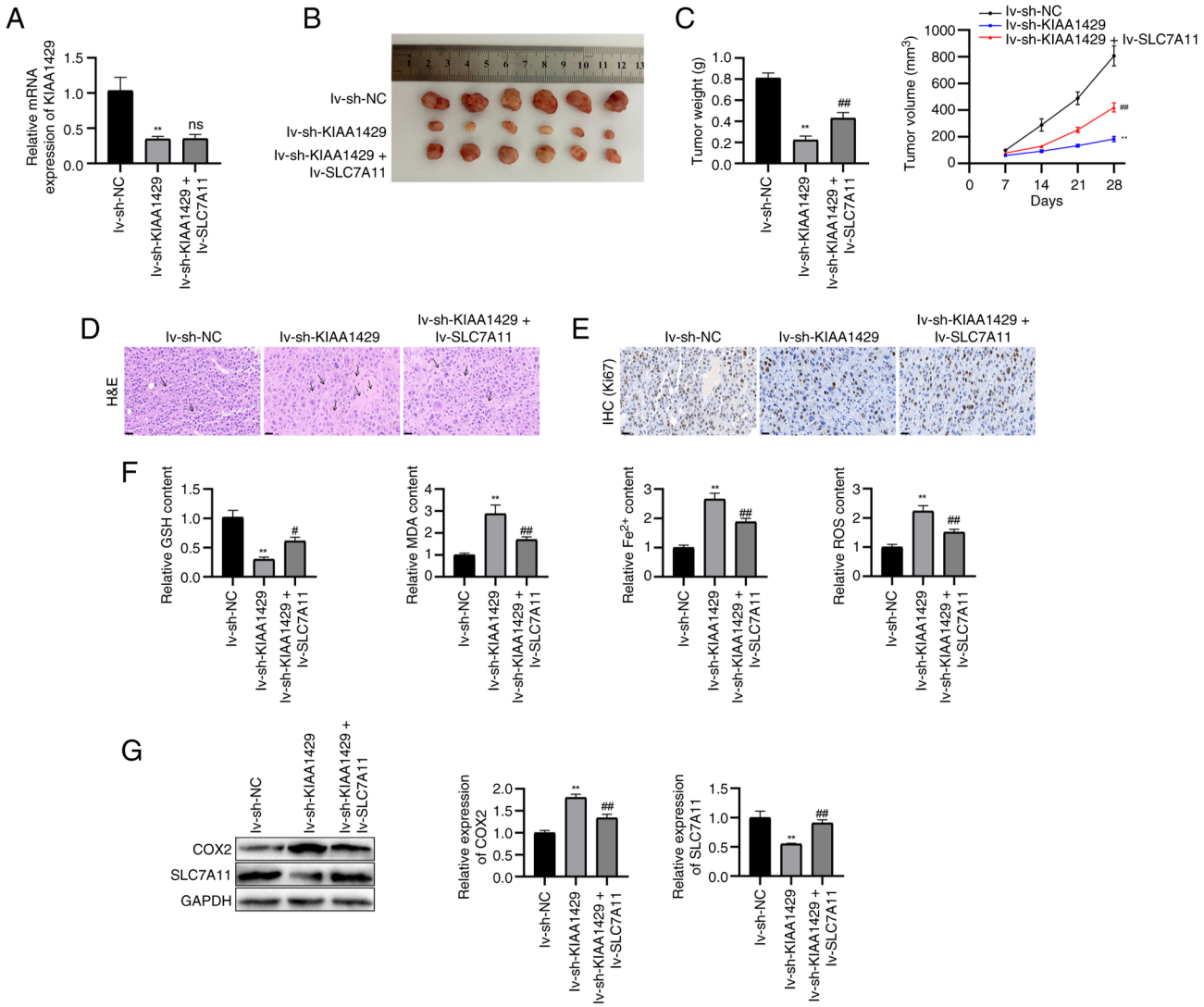

Figure 8. KIAA1429 knockdown suppresses osteosarcoma growth and ferroptosis *in vivo*. (A) Reverse transcription-quantitative PCR was performed to detect the mRNA levels of KIAA1429 in tumor tissues. (B) Subcutaneous tumor formation. (C) Tumor volume and weight quantification. (D) Histopathological analysis was observed by H&E staining (magnification, x400; scale bar, 20 μm). Arrows indicate inflammatory infiltration. (E) Proliferation marker Ki67 was observed by IHC (magnification, x400; scale bar, 20 μm). (F) Levels of oxidative stress parameters (MDA, GSH, Fe^{2+} and ROS) were evaluated by ELISA. (G) Protein expression levels of ferroptosis biomarkers were assessed by western blotting. **P<0.01 vs. lv-sh-NC; $^{\#}$P<0.05, $^{\#\#}$P<0.01 vs. lv-sh-KIAA1429. COX2, cytochrome *c* oxidase 2; GPX4, GSH peroxidase 4; GSH, glutathione; H&E, hematoxylin and eosin; IHC, immunohistochemistry; lv, lentivirus; MDA, malondialdehyde; NC, negative control; ns, not significant; ROS, reactive oxygen species; sh, short hairpin; SLC7A11, solute carrier family 7 member 11.

acetylated KIAA1429 (by TIP60) facilitates immune evasion by stabilizing lysine-specific demethylase 5B mRNA via m6A modification, thereby promoting programmed death ligand 1 expression and tumor metastasis (29). In pancreatic adenocarcinoma, KIAA1429-mediated m6A modification enhances AKT2 mRNA stability, driving malignant progression and autophagy suppression (30). In diffuse large B-cell lymphoma, KIAA1429 exerts oncogenic functions through m6A-dependent regulation of carbohydrate sulfotransferase 11, thereby activating the Hippo-YAP pathway and sustaining malignant progression (31). In colorectal cancer, KIAA1429 promotes oncogenesis through m6A-independent transcriptional repression of WEE1, and its clinicopathological relevance is underscored by its notable association with poor patient survival (32). Similarly, in OS, KIAA1429-mediated m6A modifications of the ZFPM2-AS1 transcript promote malignant progression, manifested as increased cellular proliferation, motility and invasiveness (33). Luo *et al* (34) established that KIAA1429 knockdown can exert anti-oncogenic effects in OS by disrupting Janus kinase 2/signal transducer and activator of transcription 3 signaling. The current study further revealed that downregulation of KIAA1429 led to pronounced suppression of OS cell proliferation, invasion and migration, providing strong evidence of its oncogenic role in OS.

Ferroptosis, an iron-dependent form of regulated cell death, has garnered attention as a treatment strategy against therapy-resistant cancer (11). SLC7A11, a core subunit of system Xc^-, imports cystine for GSH synthesis, thereby protecting cells against oxidative stress and ferroptosis (35). SLC7A11 overexpression is associated with chemoresistance and poor survival in OS, as it maintains redox balance and suppresses iron-dependent lipid peroxidation (36). Beyond OS, SLC7A11 dysregulation has also been observed in bladder and

ovarian cancer, where it promotes tumor resilience (37,38). In non-small cell lung cancer, tripartite motif-containing 3 acts as a tumor suppressor and inhibits tumorigenesis by promoting SLC7A11 degradation (39). CCAAT/enhancer binding protein γ suppresses ferroptosis in ovarian cancer through transcriptional regulation of SLC7A11 (40). Targeting p62 with sulforaphane enhances autolysosomal degradation of SLC7A11 in OS, as demonstrated in both *in vivo* and *in vitro* models, ultimately inducing ferroptosis and inhibiting malignant progression (41). Similarly, lysine-specific demethylase 4A depletion induces ferroptosis in OS cells by increasing H3K9me3 at the SLC7A11 promoter, thereby transcriptionally regulating SLC7A11 expression (42). In the present study, KIAA1429 silencing amplified erastin-induced ferroptosis, as evidenced by enhanced lipid peroxidation, elevated MDA, ROS and iron levels, and reduced GSH activity. Additionally, KIAA1429 knockdown reduced the m6A modification of SLC7A11 mRNA, accelerating its decay and impairing its translation. This reduction amplified ferroptotic susceptibility, which was reversed by SLC7A11 overexpression. These results are consistent with the present *in vivo* findings, showing that SLC7A11 inhibition can trigger ferroptosis and suppresses OS growth. Thus, targeting the KIAA1429/SLC7A11 axis may disrupt redox adaptation in OS.

In conclusion, the current study demonstrated that KIAA1429 was significantly upregulated in OS and that KIAA1429 knockdown suppressed tumor progression. Mechanistically, KIAA1429 can stabilize SLC7A11 mRNA via m6A modification, thereby suppressing ferroptosis. Rescue experiments confirmed that SLC7A11 overexpression reversed the antitumor effects of KIAA1429 knockdown, both *in vitro* and *in vivo*. These findings reveal that the KIAA1429/SLC7A11 axis is a critical regulator of ferroptosis and OS progression, providing a promising therapeutic target for OS treatment.

Acknowledgements

Not applicable.

Funding

The present study was funded by the Ganzhou Science and Technology + National Regional Medical Center 'Joint Program Project - General Project of Key Research and Development Program' (no. 2022-YB1446), the Jiangxi Provincial Health Commission S&T Program (no. SKJP220212369) and the Medical Leading Discipline of Ganzhou City.

Availability of data and materials

The data generated in the present study may be requested from the corresponding author.

Authors' contributions

HZ made substantial contributions to study conception and design, data acquisition and drafting the article. YZ, DZ and SX performed data acquisition and drafted the article. SZ performed data acquisition and reviewed the article. HZ and SZ confirm the authenticity of all the raw data. All the authors took part in the experiments. All the authors read and approved the final manuscript.

Ethical approval and consent to participate

All methods are reported in accordance with ARRIVE guidelines for the reporting of animal experiments. The animal experiments conformed to the Guide for the Care and Use of Laboratory Animals and were approved by the Animal Ethics Committee of Ganzhou People's Hospital (approval no. PJD2026-025-01).

Patient consent for publication

Not applicable.

Competing interests

The authors declare that they have no competing interests.

References

1. Cersosimo F, Lonardi S, Bernardini G, Telfer B, Mandelli GE, Santucci A, Vermi W and Giurisato E: Tumor-associated macrophages in osteosarcoma: From mechanisms to therapy. Int J Mol Sci 21: 5207, 2020.
2. Shoaib Z, Fan TM and Irudayaraj JMK: Osteosarcoma mechanobiology and therapeutic targets. Br J Pharmacol 179: 201-217, 2022.
3. Chen C, Xie L, Ren T, Huang Y, Xu J and Guo W: Immunotherapy for osteosarcoma: Fundamental mechanism, rationale, and recent breakthroughs. Cancer Lett 500: 1-10, 2021.
4. Jafari F, Javdansirat S, Sanaie S, Naseri A, Shamekh A, Rostamzadeh D and Dolati S: Osteosarcoma: A comprehensive review of management and treatment strategies. Ann Diagn Pathol 49: 151654, 2020.
5. Li S, Zhang H, Liu J and Shang G: Targeted therapy for osteosarcoma: A review. J Cancer Res Clin Oncol 149: 6785-6797, 2023.
6. Huang J, Guo J and Jia R: N6-methyladenosine methyltransferase component KIAA1429 is a potential target of cancer therapy. Biomolecules 14: 1319, 2024.
7. Zhang X, Li MJ, Xia L and Zhang H: The biological function of m6A methyltransferase KIAA1429 and its role in human disease. PeerJ 10: e14334, 2022.
8. Ren M, Pan H, Zhou X, Yu M and Ji F: KIAA1429 promotes gastric cancer progression by destabilizing RASD1 mRNA in an m^6A-YTHDF2-dependent manner. J Transl Med 22: 584, 2024.
9. Li N, Zhu Z, Deng Y, Tang R, Hui H, Kang Y and Rana TM: KIAA1429/VIRMA promotes breast cancer progression by m^6 A-dependent cytosolic HAS2 stabilization. EMBO Rep 24: e55506, 2023.
10. Li J, Rao B, Yang J, Liu L, Huang M, Liu X, Cui G, Li C, Han Q, Yang H, *et al*: Dysregulated m6A-related regulators are associated with tumor metastasis and poor prognosis in osteosarcoma. Front Oncol 10: 769, 2020.
11. Zhou Q, Meng Y, Li D, Yao L, Le J, Liu Y, Sun Y, Zeng F, Chen X and Deng G: Ferroptosis in cancer: From molecular mechanisms to therapeutic strategies. Signal Transduct Target Ther 9: 55, 2024.
12. Liu J, Kang R and Tang D: Signaling pathways and defense mechanisms of ferroptosis. FEBS J 289: 7038-7050, 2022.
13. Zhao J, Zhao Y, Ma X, Zhang B and Feng H: Targeting ferroptosis in osteosarcoma. J Bone Oncol 30: 100380, 2021.
14. Lin W, Wang C, Liu G, Bi C, Wang X, Zhou Q and Jin H: SLC7A11/xCT in cancer: Biological functions and therapeutic implications. Am J Cancer Res 10: 3106-3126, 2020.
15. Rochette L, Dogon G, Rigal E, Zeller M, Cottin Y and Vergely C: Lipid peroxidation and iron metabolism: Two corner stones in the homeostasis control of ferroptosis. Int J Mol Sci 24: 449, 2022.
16. Zhang L, Luo D, Ren H, Fan W, Yu Z, Wang S, Wu X, Xu Y and Li S: Brusatol induced ferroptosis in osteosarcoma cells by modulating the Keap1/Nrf2/SLC7A11 signaling pathway. Phytomedicine 144: 156912, 2025.

17. Xie C, Xiao Y, Yang L and Luo J: KIAA1429 silencing ameliorates osteosarcoma progression through promoting ferroptosis via Nrf2/NQO1 axis. Inflamm Res 74: 111, 2025.
18. Livak KJ and Schmittgen TD: Analysis of relative gene expression data using real-time quantitative PCR and the 2(-Delta Delta C(T)) method. Methods 25: 402-408, 2001.
19. Wang X, Chen Q, Bing Z, Zhou S, Xu Z, Hou Y, Zhao Y, Zhao S and Wang T: Low expression of m6A reader YTHDC1 promotes progression of ovarian cancer via PIK3R1/STAT3/GANAB axis. Int J Biol Sci 19: 4672-4688, 2023.
20. Ji FH, Fu XH, Li GQ, He Q and Qiu XG: FTO prevents thyroid cancer progression by SLC7A11 m6A methylation in a ferroptosis-dependent manner. Front Endocrinol (Lausanne) 13: 857765, 2022.
21. Wang H, Chen W, Cui Y, Gong H and Li H: KIAA1429 protects hepatocellular carcinoma cells from ferroptotic cell death with a m^6 A-dependent posttranscriptional modification of SLC7A11. J Cell Mol Med 27: 4118-4132, 2023.
22. Haynes L, Kaste SC, Ness KK, Wu J, Ortega-Laureano L, Bishop M, Neel M, Rao B and Fernandez-Pineda I: Pathologic fracture in childhood and adolescent osteosarcoma: A single-institution experience. Pediatr Blood Cancer 64: 10.1002/pbc.26290, 2017.
23. Liu H, Tian L, Mu J, He X, Zhuangzhuang L, Gong T, Wang J, Min L, Lu M and Tu C: The resection of extraosseous osteosarcoma was accompanied by the occurrence of pulmonary metastasis and distal metastasis at the primary site: A case report. Front Oncol 15: 1549722, 2025.
24. Uddin MB, Wang Z and Yang C: The m^6A RNA methylation regulates oncogenic signaling pathways driving cell malignant transformation and carcinogenesis. Mol Cancer 20: 61, 2021.
25. An Y and Duan H: The role of m6A RNA methylation in cancer metabolism. Mol Cancer 21: 14, 2022.
26. Hu T, Wang G, Wang D, Deng Y and Wang W: m6A methylation modification: Potential pathways to suppress osteosarcoma metastasis. Int Immunopharmacol 145: 113759, 2025.
27. Miao W, Chen J, Jia L, Ma J and Song D: The m6A methyltransferase METTL3 promotes osteosarcoma progression by regulating the m6A level of LEF1. Biochem Biophys Res Commun 516: 719-725, 2019.
28. Yadav P, Subbarayalu P, Medina D, Nirzhor S, Timilsina S, Rajamanickam S, Eedunuri VK, Gupta Y, Zheng S, Abdelfattah N, *et al*: M6A RNA methylation regulates histone ubiquitination to support cancer growth and progression. Cancer Res 82: 1872-1889, 2022.
29. Quan H, Zhou H, Chen F, Chen J, He Y, Xiao H, Liu J, Shi L, Xie W, Chen P and Luo J: Acetylated KIAA1429 by TIP60 facilitates metastasis and immune evasion of hepatocellular carcinoma via N6-methyladenosine-KDM5B-mediated regulation of FoxO1. Cell Death Discov 11: 210, 2025.
30. Li P, Lu Y, Zheng Z, Lv J and Hu J: The role and mechanism of KIAA1429-mediated m6A modification in pancreatic adenocarcinoma. Mol Carcinog 64: 1667-1682, 2025.
31. Chen X, Lu T, Cai Y, Han Y, Ding M, Chu Y, Zhou X and Wang X: KIAA1429-mediated m6A modification of CHST11 promotes progression of diffuse large B-cell lymphoma by regulating Hippo-YAP pathway. Cell Mol Biol Lett 28: 32, 2023.
32. Ma L, Lin Y, Sun SW, Xu J, Yu T, Chen WL, Zhang LH, Guo YC, Wang YW, Chen T, *et al*: KIAA1429 is a potential prognostic marker in colorectal cancer by promoting the proliferation via downregulating WEE1 expression in an m6A-independent manner. Oncogene 41: 692-703, 2022.
33. Zhang Y, Bao Y, Zhai H, Li C, Shi H, Gong K and Bao X: KIAA1429-mediated ZFPM2-AS1 m^6A modification promotes the proliferation, migration and invasion of osteosarcoma cells. Oncol Lett 30: 453, 2025.
34. Luo J, Wang X, Chen Z, Zhou H and Xiao Y: The role and mechanism of JAK2/STAT3 signaling pathway regulated by m6A methyltransferase KIAA1429 in osteosarcoma. J Bone Oncol 39: 100471, 2023.
35. Koppula P, Zhuang L and Gan B: Cystine transporter SLC7A11/xCT in cancer: Ferroptosis, nutrient dependency, and cancer therapy. Protein Cell 12: 599-620, 2021.
36. Guo W, Wang X, Lu B, Yu J, Xu M, Huang R, Cheng M, Yang M, Zhao W and Zou C: Super-enhancer-driven MLX mediates redox balance maintenance via SLC7A11 in osteosarcoma. Cell Death Dis 14: 439, 2023.
37. Shen L, Zhang J, Zheng Z, Yang F, Liu S, Wu Y, Chen Y, Xu T, Mao S, Yan Y, *et al*: PHGDH inhibits ferroptosis and promotes malignant progression by upregulating SLC7A11 in bladder cancer. Int J Biol Sci 18: 5459-5474, 2022.
38. Fantone S, Piani F, Olivieri F, Rippo MR, Sirico A, Di Simone N, Marzioni D and Tossetta G: Role of SLC7A11/xCT in ovarian cancer. Int J Mol Sci 25: 587, 2024.
39. Wang Z, Shen N, Wang Z, Yu L, Yang S, Wang Y, Liu Y, Han G and Zhang Q: TRIM3 facilitates ferroptosis in non-small cell lung cancer through promoting SLC7A11/xCT K11-linked ubiquitination and degradation. Cell Death Differ 31: 53-64, 2024.
40. Zhang X, Zheng X, Ying X, Xie W, Yin Y and Wang X: CEBPG suppresses ferroptosis through transcriptional control of SLC7A11 in ovarian cancer. J Transl Med 21: 334, 2023.
41. Zou Q, Zhou X, Lai J, Zhou H, Su J, Zhang Z, Zhuang X, Liu L, Yuan R, Li S, *et al*: Targeting p62 by sulforaphane promotes autolysosomal degradation of SLC7A11, inducing ferroptosis for osteosarcoma treatment. Redox Biol 79: 103460, 2025.
42. Chen M, Jiang Y and Sun Y: KDM4A-mediated histone demethylation of SLC7A11 inhibits cell ferroptosis in osteosarcoma. Biochem Biophys Res Commun 550: 77-83, 2021.